

Beyond Patches: Mining Interpretable Part-Prototypes for Explainable AI

Mahdi Alehdaghi
mahdi.alehdaghi.1@ens.etsmtl.ca
LIVIA, ILLS, Dept. of Systems
Engineering,
École de technologie supérieure
Montreal, Quebec, Canada

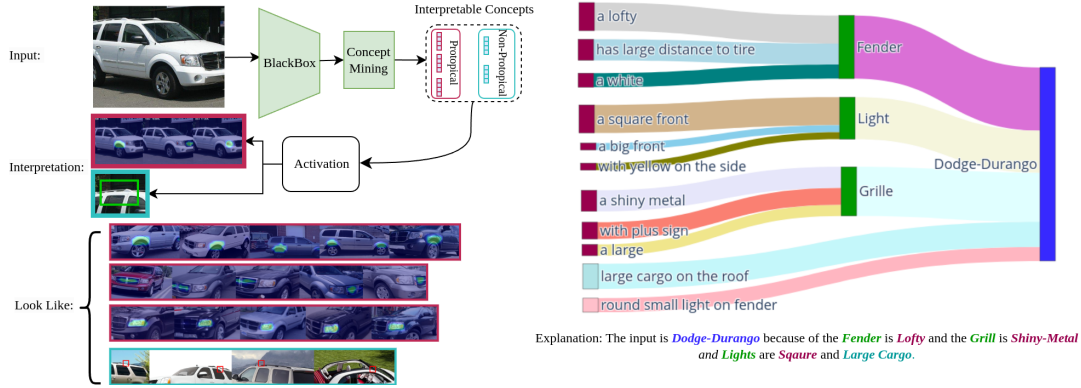
Rajarshi Bhattacharya
rajarshi.bhattacharya.1@ens.etsmtl.ca
LIVIA, ILLS, Dept. of Systems
Engineering,
École de technologie supérieure
Montreal, Quebec, Canada

Pourya Shamsolmoali
pshams55@gmail.com
Dept. of Computer Science,
University of York
York, United Kingdom

Rafael M. O. Cruz
rafael.menelau-cruz@etsmtl.ca
LIVIA, ILLS, Dept. of Systems
Engineering,
École de technologie supérieure
Montreal, Quebec, Canada

Maguelonne Heritier
mheritier@genetec.com
Genetec Inc.
Montreal, Quebec, Canada

Eric Granger
eric.granger@etsmtl.ca
LIVIA, ILLS, Dept. of Systems
Engineering,
École de technologie supérieure
Montreal, Quebec, Canada



Abstract

Deep learning has provided considerable advancements for multi-media systems, yet the interpretability of deep models remains a challenge. State-of-the-art post-hoc explainability methods, such as GradCAM, provide visual interpretation based on heatmaps but lack conceptual clarity. Prototype-based approaches, like ProtoPNet and PIPNet, offer a more structured explanation but rely on fixed patches, limiting their robustness and semantic consistency. To address these limitations, a part-prototypical concept mining network (PCMNet) is proposed that dynamically learns interpretable prototypes from meaningful regions. PCMNet clusters prototypes into concept groups, creating semantically grounded explanations without requiring additional annotations. Through a joint process of unsupervised part discovery and concept activation vector extraction, PCMNet effectively captures discriminative concepts and makes interpretable classification decisions. Our extensive experiments comparing PCMNet against state-of-the-art methods on multiple datasets show that it can provide a high level of interpretability, stability, and robustness under clean and occluded scenarios.

CCS Concepts

• **Computing methodologies** → Knowledge representation and reasoning.

Keywords

xAI, Model Interpretability, Unsupervised Concept Mining

ACM Reference Format:

Mahdi Alehdaghi, Rajarshi Bhattacharya, Pourya Shamsolmoali, Rafael M. O. Cruz, Maguelonne Heritier, and Eric Granger. 2025. Beyond Patches: Mining Interpretable Part-Prototypes for Explainable AI. In . ACM, New York, NY, USA, 13 pages. <https://doi.org/10.1145/nnnnnnn.nnnnnnn>

1 Introduction

Deep learning (DL) has revolutionized computer vision, enabling models to achieve remarkable performance across a range of tasks, from object detection to image classification. Despite these successes, the opaque nature of DL models has raised concerns regarding their interpretability and trustworthiness. In high-stakes domains such as healthcare [13], autonomous driving [17], and security [7, 24], understanding why a model makes a certain decision is as critical as the decision itself. Interpretability not only fosters trust but also aids in identifying potential biases, debugging models,

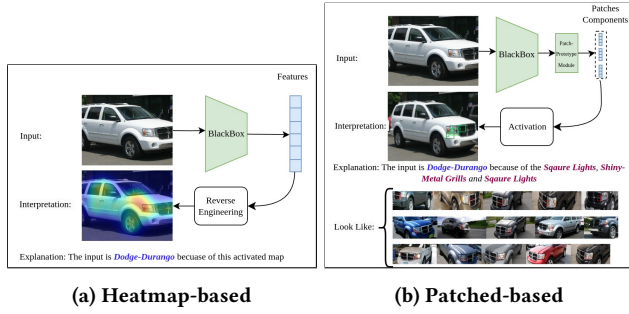


Figure 2: Explaining the decision through examples. (a) Heatmap-based methods see the feature backbones as black-box models, and try to locate regions activated by the most important features. (b) With patch-based methods, the features are decomposed into components extracted by image patches, and an explanation is provided by these components.

and ensuring compliance with ethical and legal standards. Consequently, there is a growing demand for deep vision models that are not only accurate but also capable of explaining their predictions in a clear and comprehensible manner [27, 34].

Common post-hoc explainability techniques such as GradCAM [5, 28] or ScoreCAM[36] try to interpret the model’s decision by reverse-engineering and finding the regions of the input image that contribute most to the output after the training process, as shown in Fig. 2a. In contrast to such black-box reverse-engineering methods, ante-hoc techniques [7, 23, 24, 26, 38] make the backbone produce interpretable components to explain its decision. This recognition-by-components theory [3] describes how humans recognize objects by segmenting them into multiple meaningful concepts. Some ante-hoc methods such as ProtoNet [7] and PIPNet [24], as shown in Fig. 2b, segment the spatial deep features extracted by the backbone (before the final pooling layer) into fixed, small patch components and learn a set of prototypes from them. These prototypes, activated by the patches, provide an interpretation of the model’s decision and allow users to identify and compare similar prototypes across different input images. However, these methods have significant limitations. Fixed patch sizes can lead to instability in prototype activation for larger areas, which may fail to focus on primitive semantics. Smaller patches, similarly, may also lose their interpretive capacity due to the limited area they represent. Furthermore, many discriminative and explainable attributes require larger regions to capture their semantic meaning effectively to avoid duplicating the same concept in explanation examples (two similar rows at the bottom of Fig.2b). In other words, the regions containing the prototypes can be dynamic and require training.

Direct application of naïve unsupervised part-discovery or Slot Attention-based methods often falls short in capturing primitive, semantically meaningful concepts from images and fails to provide intuitive explanations of model decisions based on extracted prototypes [21, 32]. This limitation arises because part features are typically employed merely to identify similar parts across objects, without enforcing conceptual consistency, while Slot Attention features tend to lack explicit prototypical representations required for interpretable reasoning. The result, therefore, is a reduction in the

diversity and a lack of interpretability of the prototypes, hindering the model’s ability to provide meaningful and comprehensive explanations for its decisions.

To address these limitations, this paper introduces an intrinsically interpretable image classifier that mines meaningful and interpretable prototypical concepts from dynamic regions in images to explain the model’s decisions. Our unsupervised concept mining network identifies semantically meaningful components, relying only on class labels without requiring additional part labels or annotations. Our part-prototype concept mining network (PCMNet) detects larger, coherent regions of pixels as meaningful prototype parts. This design allows the components to identify relationships between semantically similar prototypes across instances from different classes. Then, we leverage these prototypes to mine a set of primitive yet discriminative concepts used to explain the model’s reasoning directly. For instance, Figure 2 demonstrates an use case where the prototype heatmaps, derived from our pipeline, shows that the decision-making was based on the "lofty fenders", "shiny metal grille" and "square shaped lights", to conclude that the vehicle in the image, is a Dodge Durango.

In the first stage, PCMNet employs an unsupervised part discovery mechanism to learn a set of prototypes using a novel center-clustering loss. In the second stage, the model encodes the deep features into a sparse Concept Activation Vector (CAV) [16], which provides a spatially and semantically interpretable explanation of the final decision. Each concept activation is computed as the cosine similarity between part features and class-aware prototype centroids. To ensure that these activated concepts are both primitive and class-discriminative, PCMNet applies a clustering algorithm to the part features corresponding to each class-specific prototype. The center of each resulting cluster then serves as a class-aware prototype centroid. Interpretation of the resulting CAV is straightforward, as it is produced by a sparse, non-negative linear layer that guarantees all concept values remain non-negative.

The contributions of this paper are summarized as follows. **(1)** PCMNet is presented as a part-prototypical concept mining framework for explaining vision classifiers with primitive, prototypical, and interpretable human-meaningful components. **(2)** Concepts extracted by PCMNet are leveraged from a broader region than single patches to contain more semantical part-prototype abstraction, similar to the human brain, by using a novel contrastive prototype extraction. **(3)** Two-level clustering mechanisms are proposed for finding interpretable parts at the pixel level and primitive and intuitive concepts at the feature level. **(4)** Our experiments show that PCMNet explanation is more robust to occlusions, outperforming state-of-the-art patched-based prototype methods according to classification and explainability metrics.

2 Related Work

(a) Post-hoc or heatmap-based explanation: Heatmap-based explainability methods are a widely used family of post-hoc techniques that visualize which parts of an input image contribute most to a model’s decision. These techniques, often referred to as attribution methods, assign importance scores to different image regions to highlight influential features. Gradient-based methods, such as GradCAM [29] and ScoreCAM [36], generate heatmaps

by backpropagating gradients concerning input features, revealing class-specific activation regions. While GradCAM produces class-dependent heatmaps, other methods like FullGrad [31] are class-agnostic, providing a more general view of model behavior across different outputs. Despite their popularity, gradient-based methods suffer from high sensitivity to noise, which can lead to unreliable and inconsistent heatmaps. To mitigate this, gradient-free CAM techniques, such as ScoreCAM, have been proposed to generate more stable and interpretable explanation maps.

Beyond gradient-based methods, attribution propagation approaches offer an alternative way to decompose model predictions into layer-wise relevance scores. Techniques such as Layer-wise Relevance Propagation (LRP) [2] recursively distribute relevance through the network, providing a structured breakdown of model decisions. While initially designed for convolutional neural networks (CNNs), recent adaptations have extended these methods to vision transformers (ViTs) [6], leveraging their self-attention mechanisms for improved interpretability. However, despite their effectiveness in highlighting important image regions, both gradient-based and attribution propagation methods remain fundamentally limited in providing high-level, human-interpretable concepts. Unlike our proposed PCMNet, which explains decisions through part-based prototypes, heatmap-based methods do not inherently capture semantic relationships between features, making them less suitable for interpretable concept-based explanations.

Additionally, since these methods are inherently post-hoc, they do not enable real-time user intervention during test-time inference. This means that once a model makes a prediction, users cannot modify or refine the explanations interactively, limiting their practical use in applications requiring human-in-the-loop decision-making. In contrast, PCMNet introduces an ante-hoc, concept-driven interpretability approach that allows for more direct, structured, and interactive explanations by providing semantically meaningful components rather than relying solely on heatmap visualizations.

(b) Slot attention: Slot Attention has emerged as a powerful mechanism for learning object-centric representations by dynamically assigning feature regions to a fixed number of latent slots [21]. Unlike traditional attention mechanisms that distribute importance weights across all features, Slot Attention iteratively refines a small set of slots, each representing a distinct object or meaningful component of an image. This allows models to decompose scenes into structured representations without explicit supervision [19]. By leveraging iterative updates with attention-based routing, Slot Attention enables more interpretable feature learning, where each slot encapsulates a semantically meaningful part of the input. This property makes it particularly useful for explainable AI, as it provides a structured decomposition of an image, rather than relying on uninterpretable distributed feature maps [14].

Recent works have applied Slot Attention in various domains, such as object discovery, segmentation, and interpretable classification [22, 30]. In the context of explainable deep learning, it has been used to learn disentangled representations where each slot corresponds to a distinct semantic concept [15]. However, these methods typically focus on object-level decomposition rather than part-based representation. Our PCMNet builds on this idea by using Slot Attention-inspired mechanisms to discover meaningful part prototypes rather than full objects, ensuring better granularity in

concept-based explanations. By applying slot-like iterative attention within a contrastive prototype extraction framework, PCMNet refines part-based representations, making them more interpretable and aligned with human perception and reasoning.

(c) Concept-based explanation: Contrary to traditional local feature attribution methods that assess the importance of input-level features, concept-based XAI methods [2, 7, 11, 26] analyze the role of latent representations in specific layers of a deep neural network (DNN). These methods explore concepts through various mechanisms, including individual neurons, directional representations such as Concept Activation Vectors (CAVs) [16], or broader feature subspaces. Early XAI research primarily focused on understanding how these concepts contribute to global decision-making, identifying the most relevant concepts for a given output class [2, 11]. Some approaches enhance model interpretability by employing local feature attribution techniques to localize and quantify the importance of concepts for individual predictions, thereby enabling concept-based explanations at the instance level [23, 24]. While these methods provide faithful explanations aligned with the model's internal reasoning, they are vulnerable to performance degradation under occlusion, as their extracted concepts often rely on limited and highly localized discriminative regions of the input. PCMNet addresses this limitation by part-based prototypical concept reasoning to rely on other discriminative parts that are not occluded.

Additionally, although instance-wise concept-based explanations provide deeper insights, they can also be overwhelming and difficult for stakeholders to process, as hundreds of concepts may need to be analyzed for each instance. To address this, some works highlight the benefits of visualizing local decisions within a global embedding space [10, 11]. With PCMNet, we build upon this idea by introducing part prototypes that encapsulate local concepts. This approach reduces the cognitive load for human interpretation by enabling comparisons between individual (local) prediction and prototypical concepts, making explanations more intuitive and structured.

3 Proposed Prototypical Concept Mining Network

To explain the decision for a classification problem with a training set \mathcal{T} containing N images $\{(x^1, y^1), \dots, (x^N, y^N)\} \in \mathcal{X} \times \mathcal{Y}$, with L classes, the PCMNet extracts primitive and sparse concepts that are activated and discriminate the object. These concepts are described in a limited set of prototypes that existed for almost all images in the datasets (e.g., lights, fenders, and grilles for cars or heads and wings for birds). In other words, the output of our model is the activated concept vector $z_i = [z_p^i]_{p=1}^K$, in which p is the prototype index. Fig. 3 shows the overall overview of our approach.

PCMNet transforms features extracted from the backbone model into explainable and interpretable concepts in three steps. **Step 1:** The model finds semantically independent, meaningful regions from input images in an unsupervised way by minimizing our novel Marginal Cluster Center loss to learn the prototypes that describe these parts. Then, the part features are disentangled to discriminate the class label. **Step 2:** Once the part features are learned for the training data, for each part inside all instances of each class, a set of shared elementary characteristics is found by applying a

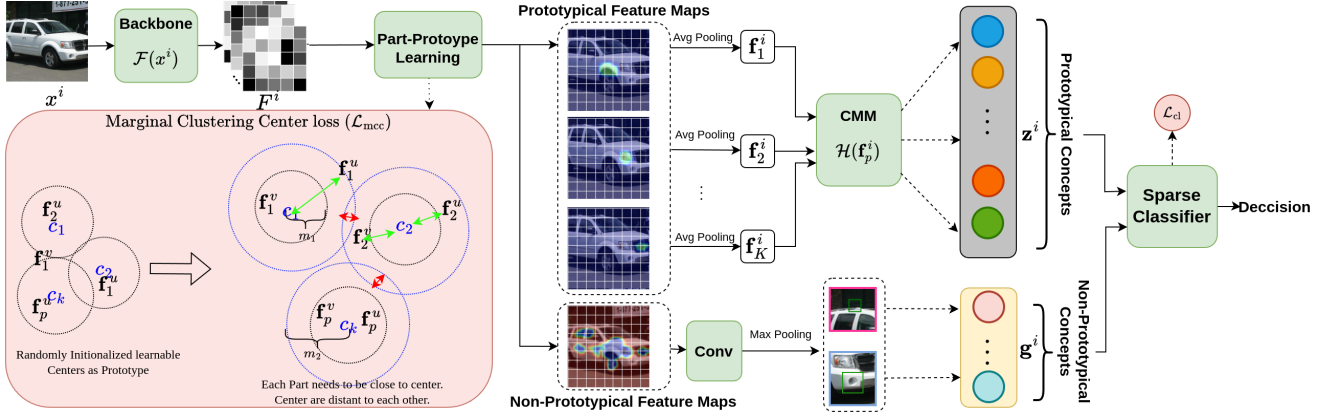


Figure 3: Overall architecture of PCMNet. In the first stage, part prototypes are learned from spatial features extracted by the backbone. In the second stage, prototypes are clustered within each class to identify frequently occurring concepts. The center of these clusters is computed as concept prototypes, and the distance between part prototypes and concept clusters determines the activated concepts for the model’s decision-making. This approach enables interpretable and concept-driven classification.

clustering approach to these features. Then, the centroid list, which represents the prototypical concepts, is generated by calculating the center of each cluster. **Step 3:** Extract the Concept Activation Vector (CAV) for the generated centroid list by computing the similarity of extracted features and each centroid. The CAVs are used to discriminate the class of the input and explain the decision. Also, to avoid losing some discriminative concepts that are not prototypical (i.e., specific and unique for this class and not available for others), we combine the features that are located outside of prototypical maps into the CAVs for classification.

3.1 Step 1: Part-Prototype Discovery

Our model is shown in Fig. 3. The input images are given to a backbone to extract the 3D deep features as $F^i \in \mathbb{R}^{D \times w \times h}$ where D is the channel size and w, h denotes the width and height. Based on extracted deep features F^i , our model finds semantically independent meaningful regions that can be shared in different inputs. We name them “part-prototype”. For determining regions, the model scores each pixel in F^i to specify their belongingness to each part-prototype class. The mapping score for each pixel in the location (q) is represented by M^i , we have $\sum_{p=1}^{K+1} M_p^i(q) = 1$. The spatial feature for each part, f_p^i , is computed by element-wise multiplication of M_p^i to F^i . The part features, f_p^i is computed as:

$$f_p^i = \mathcal{GP}(\text{conv}(F_p^i)) \in \mathbb{R}^{d_f}, \quad (1)$$

where \mathcal{GP} is the global average pooling and d_f is the dimension of features. The last index ($K+1$) is used to cover the background or non-part regions of the foreground [1]. We name these features non-prototypical concepts that are computed as:

$$g^i = \mathcal{MP}(\text{conv}(F_{K+1}^i)) \in \mathbb{R}^{d_f}, \quad (2)$$

where \mathcal{MP} is the max-pooling. We use the PDiscoNet [32] as the baseline for extracting parts features. Our part loss comprises their final loss (\mathcal{L}_{bl}) without their orthogonal component and our marginal cluster center loss (\mathcal{L}_{mcc}):

$$\mathcal{L}_{\text{part}} = \mathcal{L}_{bl} + \alpha \mathcal{L}_{mcc}. \quad (3)$$

The goal of \mathcal{L}_{mcc} is to ensure the selected region for each part remains consistent across all inputs and serves as a prototype; it must capture similar semantic information across different classes. Additionally, these sub-part features should be both class-descriptive and contain unique ID-aware information.

3.1.1 Marginal Cluster Center Loss. We proposed learnable prototypes as features to be distant from each other and then pushed the model to discover the parts from input images to be close to these prototypes. A soft margin is used to make space for the same part from input images with different classes.

$$\mathcal{L}_{mcc} = \sum_{p=1}^K [||f_p^i - c_p|| - m_1]_{\star} + \frac{1}{K} \sum_{q=p+1}^K [m_2 - ||c_p - c_q||]_{\star}, \quad (4)$$

where c_p is a learnable prototype for part p and $[\cdot]_{\star} = \max(\cdot, 0)$.

3.2 Step 2: Part-Centroid List Generation

During training in Step 1, the backbone learns to extract and use part-prototype features from the input data to fulfill its training task. To find all relevant spatial and class-aware concepts, as shown at the top of Fig. 4, we collect all extracted features from the backbone for each class and each part and then cluster them to have a minimal set of plain concepts that consistently describe the visual attributes of those parts. Multiple concepts are considered. They can be seen in each part of each class for more complex objects. To mine those concept prototypes, the centroids of each cluster are computed as $C(l, p, j) \in \mathbb{R}_f^d$ for a clustering index of l , part p , and a class of j .

3.3 Step 3: Concept Activation Mining

Once the centroid list is generated, each concept’s activation value is defined by the similarity of extracted features to each centroid:

$$z^i = [\mathcal{S}(C(l, p, j), f_p^i) \forall p \in \{1..K\} \text{ and } j \in \{1..L\}] \in \mathbb{R}^{d_c} \quad (5)$$

where \mathcal{S} is cosine distance and $[\cdot]$ represents the vector concatenation. d_c is the number of total concept centroids. We aim to explain each output class of our model using a small set of interpretable concepts. We, therefore, train a sparse classifier on top of z^i to

obtain the final classification scores $o^i = W_1^T z^i + W_2^T g^i + b$ and the predicted class $\hat{y}^i = \arg \max(o^i)$. Here, $W_1 \in \mathbb{R}^{d_c \times L}$, $W_2 \in \mathbb{R}^{d_f \times L}$ and $b \in \mathbb{R}^L$ denote the classification weights and bias term, respectively. This layer is trained with the following classification loss, using the GLM-SAGA optimizer [37]:

$$\mathcal{L}_{cl} = \mathcal{L}_{ce}(W_1^T z^i + W_2^T g^i + b, y^i) + \lambda \mathcal{R}(W_1), \quad (6)$$

where \mathcal{L}_{ce} is the cross-entropy loss, y^i is the label, λ is the sparsity regularization strength and $\mathcal{R}(W) = (1 - \gamma) \frac{1}{2} \|W\|_F + \gamma \|W\|_1$, here $\|W\|_F$ is the Frobenius norm and $\|W\|_1$ is the element-wise matrix.

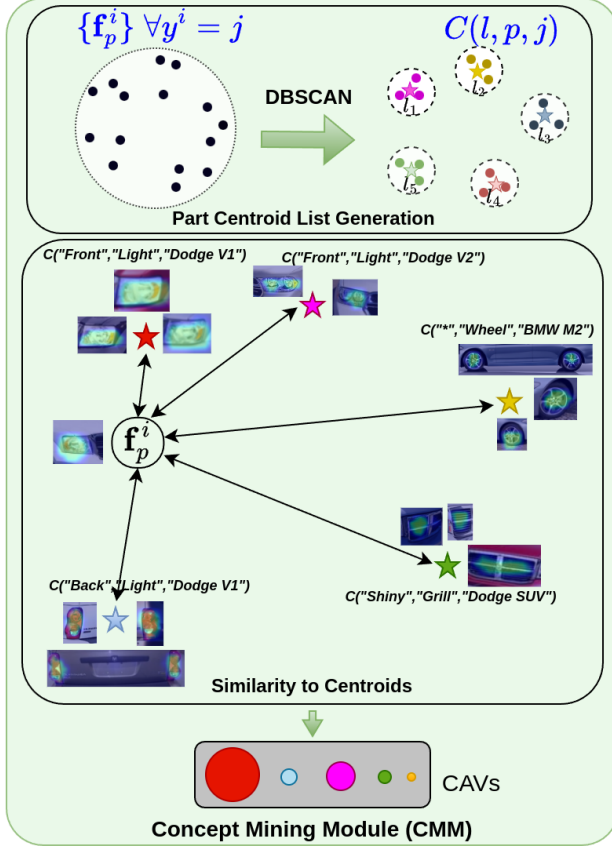


Figure 4: Concept Mining Module. First, a part centroid list is generated by applying DBSCAN[12] clustering within each class and computing the centers of the resulting clusters. These centroids serve as frequently occurring concept prototypes. Next, to activate the most relevant concept for a given part feature, the similarity (inverse distance) to the centroids is measured. These values are then used as CAVs to inform the model’s decision-making process .

3.4 Overall Training

We jointly optimize the network in an end-to-end manner by loss:

$$\mathcal{L} = \mathcal{L}_{part} + \beta \mathcal{L}_{cl}, \quad (7)$$

where β is hyperparameter. For the first step of training, we set $\beta = 0$; then, once the part-prototypical concepts are learned, we set $\beta = 2$ based on our hyperparameter analysis.

4 Experiments and Results

PCMNet is validated on standard benchmarks in prototype literature: Stanford Cars [20] (196 classes of different make and models) and CUB-200-2011 [35] (200 bird species, including attribute annotation for visual features). The ResNet50 model pretrained on ImageNet [9] is used as the feature backbone. Each training batch (32 images) is resized to 488×488 , randomly cropped, erased, and padded. Optimization follows ADAM [18] with a linear warm-up. We set regularization parameters λ and γ as same in [25]. $\alpha = 1.5$, $\beta = 2$, with $m_1 = 0.3$ and $m_2 = 1.5$ chosen via hyperparameter analysis in the suppl. material. More details on the experimental protocol are presented in the supplementary materials.

4.1 Explainability Metrics

To evaluate the explainability of final features, we rely on performance metrics established in the literature [11] with some minor modifications to express better comprehension.

(a) Faithfulness: Faithfulness[4, 8] evaluates how much the activated concepts influence the model’s final prediction, serving as a key metric for assessing the quality of explanations. One widely used approach for measuring faithfulness is concept deletion, which involves removing selected concepts from the model’s reasoning process and observing the resulting change in output confidence. Prior works, such as [11], typically assess this by removing only the single most important concept. However, this limited scope fails to capture the broader contribution of other activated concepts and may not reveal the full extent of their impact. To provide a more comprehensive assessment, we extend this approach by successively removing the top- k most activated concepts and measuring the resulting drop in model confidence. A larger drop indicates higher faithfulness, as it suggests that the removed concepts were indeed critical to the model’s decision. This extended evaluation allows us to better quantify how much the explanation aligns with the model’s internal reasoning.

(b) Stability: The extracted concepts from input images that share some semantic concepts must be stable and explainable for unseen images. To evaluate stability, we compute CAVs on k -fold subsets of the data ($k = 10$ as default) similar to [11] for all classes at steps 2 and 3. We then map CAVs together using a Hungarian loss function and measure the cosine similarity between them.

(c) Consistency: Activated concepts from images with the same class should be similar to be consistent and explain the model’s decision. To measure this consistency, we extract the CAV from images and then measure the cosine similarity between them. The mean cosine similarity is assessed between images from the same class and between images from different classes. The ratio between inter/intra-class similarity should be high for a stable explanation.

(d) Sparseness: The sparseness metric essentially describes the uniformity of the concept activation, where having some concepts activate more than others is considered easier to interpret. This is because a uniform distribution of concept activations would provide

	Method	Consistency (Intra) \uparrow	Consistency (Inter) \downarrow	F(1)-F(5) \uparrow	Sp \uparrow	Stability	C Acc \uparrow
Stanford Cars	Resnet50+Act	83.45 \pm 2.7	27.26 \pm 28.10	0.16 - 0.23	22.74	65.4	84.1
	Resnet50+W \times Act	83.45 \pm 2.7	27.26 \pm 28.10	1.54 - 6.61	22.74	65.4	84.1
	ProtoPNet + Act	45.70 \pm 4.9	11.22 \pm 5.5	2.2-55.64	60.92	69.6	84.5
	ProtoPNet + W \times Act	45.70 \pm 4.9	11.22 \pm 5.5	9.3-80.12	60.92	69.6	84.5
	PiPNet(Covx) + Act	52.78 \pm 7.4	9.07 \pm 9.4	0.02-60.62	70.59	65.2	88.5
	PiPNet(Covx) + W \times Act	52.78 \pm 7.4	9.07 \pm 9.4	10.83- 95.66	70.59	65.2	88.5
	PiPNet(Res50) + Act	42.40 \pm 17.5	17.4 \pm 2.4	0.18 - 1.21	63.19	60.8	86.46
	PiPNet(Res50) + W \times Act	42.40 \pm 17.5	17.4 \pm 2.4	9.43 - 93.15	63.19	60.8	86.46
	Ours + Act	55.32 \pm 6.1	1.88 \pm 9.37	37.94 - 63.3	57.45	71.5	88.7
	Ours + W \times Act	55.32 \pm 6.1	1.88 \pm 9.37	59.33 - 91.73	57.45	71.5	88.7
Birds (CUB 200)	Resnet50+Act	57.38 \pm 3.50	25.45 \pm 23.82	0.35 - 1.12	24.14	60.3	81.2
	Resnet50+Rel \times Act	57.38 \pm 3.50	25.45 \pm 23.82	2.43 - 5.73	24.14	60.3	81.2
	ProtoPNet + Act	51.47 \pm 5.8	10.16 \pm 9.2	1.15-51.96	79.51	63.6	81.45
	ProtoPNet + W \times Act	51.47 \pm 5.8	10.16 \pm 9.2	9.36-75.50	79.51	63.6	81.45
	PiPNet(Covx) + Act	54.80 \pm 8.3	7.77 \pm 8.0	0.01-54.14	80.72	64.7	85.0
	PiPNet(Covx) + W \times Act	54.80 \pm 8.3	7.77 \pm 8.0	5.13-92.83	80.72	64.7	85.0
	PiPNet(Res50) + Act	42.28 \pm 3.2	15.57 \pm 15.7	0.14 - 2.35	77.83	65.9	82.0
	PiPNet(Res50) + W \times Act	42.28 \pm 3.2	15.57 \pm 15.7	9.40 - 89.77	77.83	65.9	82.0
	PCMNNet (Ours) + Act	58.55\pm7.5	1.22 \pm 10.1	41.82 - 75.24	57.45	67.1	84.7
	PCMNNet (Ours) + W \times Act	58.55\pm7.5	1.22 \pm 10.1	55.13 - 89.88	57.45	67.8	84.7

Table 1: Performance of PCMNNet according to xAI metrics on the Stanford Cars and Birds datasets.

little information on the importance of specific concepts or parts of the images, i.e., a high entropy in the generated concepts.

4.2 Comparison to Prototype xAI Methods

To evaluate PCMNNet, we report the classification accuracy and the XAI evaluation criteria discussed in Sec 4 and compare them to other ante-hoc methods (ProtoPNet[7] and PiPNet[24]) in tables 1. The consistency metric is reported in two ways: Intra and Inter, which are cosine similarities between activated concepts of the same class and different classes, respectively. Faithfulness is reported as $F(n)$, measuring accuracy drops when the top n important concepts are removed from the decision. To compute the contribution of each concept or feature to the final decision, we evaluate two strategies: (1) using raw values of each concept ("Act"), and (2) computing a weighted contribution (gradient) as the product of raw values and its corresponding weight in the classification layer ("W \times Act").

4.3 Ablation Studies

4.3.1 Number of Prototypes. We assess the impact of the number of parts on both classification accuracy and faithfulness in Table 2. As the model extracts more prototypical concepts, its decisions become more aligned with the underlying features, enhancing interpretability. Interestingly, when the number of prototypes is smaller, the faithfulness scores for the top concepts tend to be higher. This is because the model relies on a more compact set of prototypes, concentrating its decisions on fewer, more influential concepts.

4.3.2 Effect of Modules. To evaluate the effectiveness of each component in PCMNNet, we conduct an ablation study on the baseline PDiscoNet model, which extracts local parts without explicit concept learning. As shown in Table 3, we analyze classification accuracy (C Acc) and feature faithfulness under occlusion (F(3)) on

both the Cars and Birds datasets, alongside the model size and FLOPs. Introducing the Marginal Clustering Center (MCC) loss into the baseline improves classification performance (from 84.2% to 86.1% on Cars) and more than doubles faithfulness scores, indicating that enforcing clustering consistency across part features supports more explainability. The inclusion of the Concept Mining Module (CMM)—responsible for extracting sparse and interpretable concepts—dramatically boosts faithfulness (from 4.9% to 55.6% on Birds), even with minimal impact on accuracy. When both MCC and CMM are combined, PCMNNet achieves the best results across all metrics, including 87.5% classification accuracy and 67.4% faithfulness on Cars, with only a marginal increase in parameter count and computational cost. These findings underscore the complementary roles of MCC in enforcing cluster-level consistency and CMM in mining high-quality, human-aligned concepts.

K value	Cars		Birds	
	C Acc	F(1)-F(5)	C Acc	F(1)-F(5)
0 (Resnet50)	84.1	1.54 - 6.61	83.2	1.21-5.56
4	83.5	79.96 - 91.01	83.5	71.42-85.64
5	84.1	70.11 - 91.33	84.9	66.7 - 85.9
6	85.2	66.02 - 90.65	85.7	59.9 - 86.7
7	86.7	62.47 - 91.25	86.0	55.7 - 87.3
8	87.5	59.33 - 91.73	85.1	53.0 - 86.4
9	86.4	55.10 - 91.52	84.4	52.5-86.1

Table 2: Impact on performance of the number of prototypes.



Figure 5: Visualizing activated concepts in the test set and examples from the training set for Stanford Cars and CUB datasets.

Settings	Cars		Birds		#Params	FLOPs
	C Acc	F(3)	C Acc	F(3)		
Baseline[32]	81.2	5.4	82.3	4.9	27.1M	17.2G
Base + MCC	86.1	9.6	84.5	9.1	27.2M	17.2G
Base + CMM	84.3	59.2	82.1	55.6	27.4M	17.5G
Base + MCC + CMM	87.5	67.4	84.7	64.9	27.5M	17.5G
PipPNet(Resnet)	86.4	62.7	82.0	58.6	25.1M	27.6G
PipPNet(Covx)	88.5	60.6	85.0	57.5	29.3M	32.3G
ProtoPNet	84.5	38.6	81.4	31.7	28.9M	18.4G

Table 3: Classification accuracy and faithfulness using different PCMNet modules.

4.4 Robustness to Occlusion

To evaluate the robustness of PCMNet’s decision-making under occlusion, we conducted controlled experiments in which regions corresponding to the most activated concepts were systematically masked, and the resulting images were re-evaluated by the model. This experiment aims to assess the stability of model predictions when key interpretable regions are removed. Specifically, we identify the center of the most activated concept—based on the model’s response to clean images—using the concept representation (patch for PIPNet and ProtoPNet, mask for PCMNet), and then occlude a

rectangular region centered around this point. We consider three levels of occlusion, masking 10%, 20%, and 30% of the image area. PCMNet’s performance under these conditions is compared against two other interpretable baselines: ProtoPNet [7] and PIPNet [24].

Fig. 7 shows that PCMNet maintains stable accuracy at lower occlusion levels and degrades more gradually than ProtoPNet and PIPNet. This resilience stems from PCMNet’s broader part-based concepts, which introduce redundancy and enable accurate predictions even when key components are missing. Unlike patch-based models that rely on fixed, small regions, it extracts prototypes from semantically meaningful, wider regions. As a result, such methods experience sharp performance drops under occlusion due to their dependence on localized patterns, whereas PCMNet remains more robust by leveraging multiple related part concepts, preventing performance from relying too heavily on a single visual cue.

4.5 Qualitative Results

4.5.1 Concept Activation and Occlusion Robustness. To further illustrate the interpretability and robustness of PCMNet, we compare the activated concepts of our method with PIPNet [24] under clean and occluded conditions, as visualized in Fig. 5. For each method, we select two activated concepts on test images and retrieve training

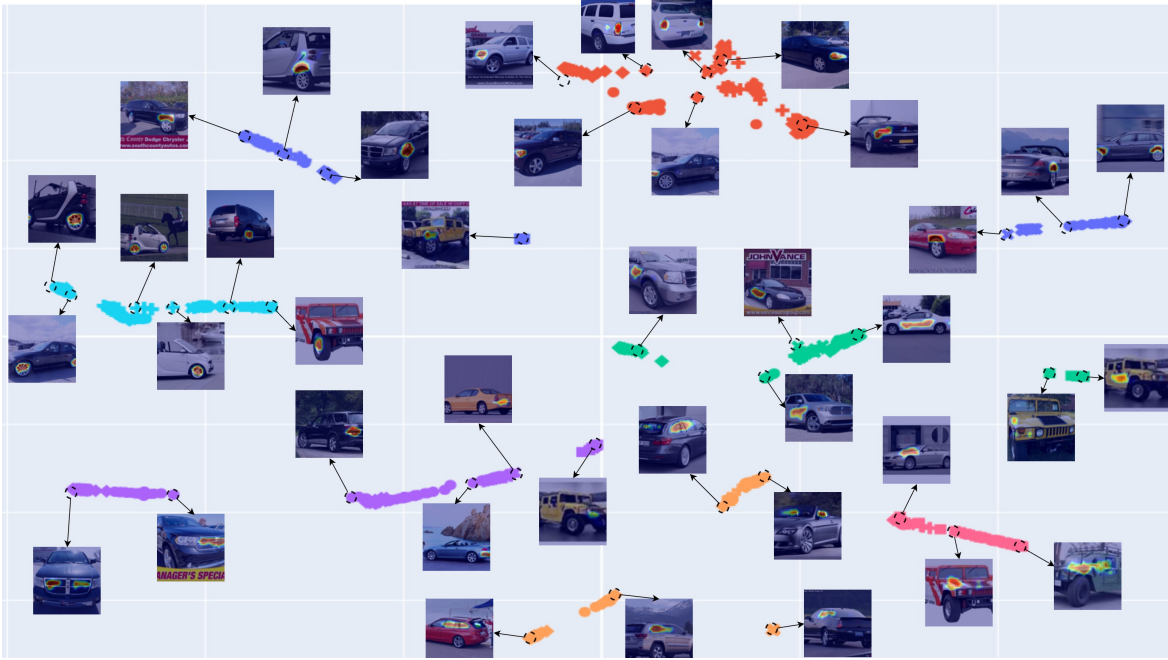


Figure 6: t-SNE visualization of concept-level part features extracted by PCMNet. Colors represent different prototypes, while shapes indicate object classes.

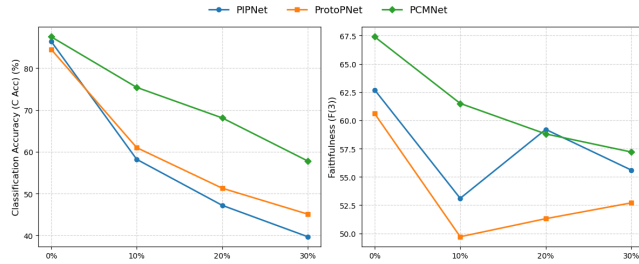


Figure 7: Classification Accuracy and Faithfulness under Different Occlusion Levels.

set examples with the highest activation values for those concepts. This comparison shows several key advantages of PCMNet:

Broader Concept Coverage: PCMNet extracts more diverse and semantically rich concepts compared to PIPNet. Our method leverages attention-based masks instead of fixed patches to capture part-level semantics over a broader spatial context, leading to more varied and interpretable regions across different object parts.

More Informative Examples: The training examples retrieved by PCMNet for each concept exhibit more clearly activated and semantically aligned regions. This suggests that the discovered concepts better reflect the underlying factors influencing the model’s decision, thereby enhancing explanation quality.

Robustness to Occlusion: Under occlusion, PIPNet often fails to highlight meaningful or consistent regions due to its reliance on limited regions. In contrast, PCMNet maintains interpretability by activating alternative, unoccluded parts that belong to the same or

related concepts. This demonstrates the model’s ability to generalize concept reasoning even when certain visual cues are missing.

4.5.2 Visualization of Concept Prototypes. To better understand the behavior of the learned prototypes in PCMNet, we visualize the extracted part-level features using t-SNE [33], as shown in Figure 6. Each point corresponds to a feature from a localized part, colors indicating the prototype (i.e., concept) and marker shapes denoting the object class. This visualization represents several insights:

Disentanglement of Prototypes: Features assigned to different prototypes form well-separated clusters, suggesting that PCMNet effectively disentangles the latent interpretable part-based concept space. This separation implies that the Marginal Clustering Center loss and Concept Mining Module (CMM) encourages diverse and semantically distinct part concepts, which supports both interpretability of model decisions and robustness on occlusion.

Multi-Class Concept Coverage: Many prototype clusters contain the same semantic parts from multiple object classes. This indicates PCMNet learns class-agnostic concepts such as lights, wheels, or windows, which are shared across different categories. Such generalization is crucial for explainability, as it facilitates human-aligned, semantically meaningful concepts that transcend dataset labels.

Intra-Class Concept Diversity: Interestingly, features from the same class are distributed across multiple prototype clusters. This highlights PCMNet’s ability to capture *intra-class variation* through multiple part-based concepts. For instance, different views or structural variations of a car class may be assigned to distinct concepts (Backlight vs headlight), further enhancing the model’s fine-grained interpretability based on human perception and explanation.

5 Conclusion

We presented PCMNet, a novel framework designed to bridge the gap between accuracy and interpretability in deep learning models. By mining part-prototypes from dynamic image regions, PCMNet improves upon existing patch-based prototype models by ensuring semantic coherence across instances. Our results show that PCMNet enhances faithfulness, concept stability, and explainability, outperforming existing interpretable models such as ProtoPNet and PIPNet. Moreover, our occlusion-based robustness analysis confirmed that PCMNet remains stable under missing or distorted input regions, demonstrating its reliability in real-world scenarios. Unlike conventional post-hoc explainability methods, PCMNet allows for more human-aligned, concept-based reasoning, making deep learning decisions more transparent and interpretable.

References

- [1] Mahdi Alehdaghi, Pourya Shamsolmoali, Rafael MO Cruz, and Eric Granger. Bidirectional multi-step domain generalization for visible-infrared person re-identification. In *2025 IEEE/CVF Winter Conference on Applications of Computer Vision (WACV)*, pages 763–773. IEEE, 2025.
- [2] Sebastian Bach, Alexander Binder, Grégoire Montavon, Frederick Klauschen, Klaus-Robert Müller, and Wojciech Samek. On pixel-wise explanations for non-linear classifier decisions by layer-wise relevance propagation. *PLoS one*, 10(7): e0130140, 2015.
- [3] Irving Biederman. Recognition-by-components: a theory of human image understanding. *Psychological review*, 94(2):115, 1987.
- [4] Chun Sik Chan, Huanqi Kong, and Guanqing Liang. A comparative study of faithfulness metrics for model interpretability methods. *arXiv preprint arXiv:2204.05514*, 2022.
- [5] Aditya Chattopadhyay, Anirban Sarkar, Prantik Howlader, and Vineeth N Balasubramanian. Grad-cam++: Generalized gradient-based visual explanations for deep convolutional networks. In *2018 IEEE winter conference on applications of computer vision (WACV)*, pages 839–847. IEEE, 2018.
- [6] Hila Chefer, Shir Gur, and Lior Wolf. Transformer interpretability beyond attention visualization. In *Proceedings of the IEEE/CVF Conference on Computer Vision and Pattern Recognition (CVPR)*, 2021.
- [7] Chaofan Chen, Oscar Li, Daniel Tao, Alina Barnett, Cynthia Rudin, and Jonathan K Su. This looks like that: deep learning for interpretable image recognition. *Advances in neural information processing systems*, 32, 2019.
- [8] Sanjoy Dasgupta, Nave Frost, and Michal Moshkovitz. Framework for evaluating faithfulness of local explanations. In *International Conference on Machine Learning*, pages 4794–4815. PMLR, 2022.
- [9] Jia Deng, Wei Dong, Richard Socher, Li-Jia Li, Kai Li, and Li Fei-Fei. Imagenet: A large-scale hierarchical image database. In *2009 IEEE conference on computer vision and pattern recognition*, pages 248–255. Ieee, 2009.
- [10] Jon Donnelly, Alina Jade Barnett, and Chaofan Chen. Deformable protopnet: An interpretable image classifier using deformable prototypes. In *Proceedings of the IEEE/CVF conference on computer vision and pattern recognition*, pages 10265–10275, 2022.
- [11] Maximilian Dreyer, Reduan Achitab, Wojciech Samek, and Sebastian Lapuschkin. Understanding the (extra-)ordinary: Validating deep model decisions with prototypical concept-based explanations. In *2024 IEEE/CVF Conference on Computer Vision and Pattern Recognition Workshops (CVPRW)*, pages 3491–3501, 2024.
- [12] Martin Ester, Hans-Peter Kriegel, Jorg Sander, Xiaowei Xu, et al. A density-based algorithm for discovering clusters in large spatial databases with noise. In *kdd*, pages 226–231, 1996.
- [13] Jean-Marc Fellous, Guillermo Sapiro, Andrew Rossi, Helen Mayberg, and Michele Ferrante. Explainable artificial intelligence for neuroscience: behavioral neurostimulation. *Frontiers in neuroscience*, 13:1346, 2019.
- [14] Klaus Greff, Siebe Van Steenkiste, and Jürgen Schmidhuber. Binding in modular neural networks. *arXiv preprint arXiv:2006.01882*, 2020.
- [15] Paulius Karazija, Katja Dorr, Michaela Perrot, Mgle Staniute, and Dominic Ritchie. Clevr-tex: A visual reasoning dataset for object-centric representations. In *Proceedings of the IEEE/CVF Conference on Computer Vision and Pattern Recognition (CVPR) Workshops*, 2021.
- [16] Been Kim, Martin Wattenberg, Justin Gilmer, Carrie Cai, James Wexler, Fernanda Viegas, et al. Interpretability beyond feature attribution: Quantitative testing with concept activation vectors (tcav). In *International conference on machine learning*, pages 2668–2677. PMLR, 2018.
- [17] Hong-Sik Kim and Inwhae Joe. An xai method for convolutional neural networks in self-driving cars. *PLoS one*, 17(8):e0267282, 2022.
- [18] Diederik P Kingma and Jimmy Ba. Adam: A method for stochastic optimization. *arXiv preprint arXiv:1412.6980*, 2014.
- [19] Thomas Kipf, Siebe van Steenkiste, Klaus Greff, Francesco Locatello, Jürgen Schmidhuber, and Olivier Bachem. Conditional object-centric learning from video. In *International Conference on Learning Representations (ICLR)*, 2022.
- [20] Jonathan Krause, Michael Stark, Jia Deng, and Li Fei-Fei. 3d object representations for fine-grained categorization. In *Proceedings of the IEEE international conference on computer vision workshops*, pages 554–561, 2013.
- [21] Francesco Locatello, Dirk Weissenborn, Thomas Unterthiner, Aravindh Mahendran, Georg Heigold, Jakob Uszkoreit, and Thomas Kipf. Object-centric learning with slot attention. In *Advances in Neural Information Processing Systems (NeurIPS)*, 2020.
- [22] Daniel Monet, Klaus Greff, Siebe Van Steenkiste, Francesco Locatello, and Olivier Bachem. Object-centric learning with slot-based attention. In *International Conference on Learning Representations (ICLR)*, 2021.
- [23] Meike Nauta, Ron Van Bree, and Christin Seifert. Neural prototype trees for interpretable fine-grained image recognition. In *Proceedings of the IEEE/CVF conference on computer vision and pattern recognition*, pages 14933–14943, 2021.
- [24] Meike Nauta, Jörg Schlöterer, Maurice Van Keulen, and Christin Seifert. Pip-net: Patch-based intuitive prototypes for interpretable image classification. In *Proceedings of the IEEE/CVF Conference on Computer Vision and Pattern Recognition*, pages 2744–2753, 2023.
- [25] Tuomas Oikarinen, Subhro Das, Lam M Nguyen, and Tsui-Wei Weng. Label-free concept bottleneck models. *arXiv preprint arXiv:2304.06129*, 2023.
- [26] Dawid Rymarczyk, Lukasz Struski, Jacek Tabor, and Bartosz Zieliński. Protop-share: Prototypical parts sharing for similarity discovery in interpretable image classification. In *Proceedings of the 27th ACM SIGKDD Conference on Knowledge Discovery & Data Mining*, pages 1420–1430, 2021.
- [27] A Saranya and R Subhashini. A systematic review of explainable artificial intelligence models and applications: Recent developments and future trends. *Decision analytics journal*, 7:100230, 2023.
- [28] Ramprasaath R Selvaraju, Michael Cogswell, Abhishek Das, Ramakrishna Vedantam, Devi Parikh, and Dhruv Batra. Grad-cam: Visual explanations from deep networks via gradient-based localization. In *Proceedings of the IEEE international conference on computer vision*, pages 618–626, 2017.
- [29] R R Selvaraju, M Cogswell, A Das, R Vedantam, D Parikh, and D Batra. Grad-cam: Visual explanations from deep networks via gradient-based localization. In *Proceedings of the IEEE International Conference on Computer Vision (ICCV)*, 2017.
- [30] Sumeet Singh, Yizheng Li, Sayna Ebrahimi, Trevor Darrell, Alexei A. Efros, and Jitendra Yu. Illiterate dall-e learns to compose. In *European Conference on Computer Vision (ECCV)*, 2022.
- [31] Suraj Srinivas and Francois Fleuret. Full-gradient representation for neural network visualization. In *Advances in Neural Information Processing Systems (NeurIPS)*, 2019.
- [32] Robert van der Klis, Stephan Alaniz, Massimiliano Mancini, Cassio F Dantas, Dino Ienco, Zeynep Akata, and Diego Marcos. Pdisconet: Semantically consistent part discovery for fine-grained recognition. In *Proceedings of the IEEE/CVF International Conference on Computer Vision*, pages 1866–1876, 2023.
- [33] Laurens van der Maaten and Geoffrey Hinton. Visualizing data using t-sne. *Journal of Machine Learning Research*, 9(86):2579–2605, 2008.
- [34] Giulia Vilone and Luca Longo. Explainable artificial intelligence: a systematic review. *arXiv preprint arXiv:2006.00093*, 2020.
- [35] Catherine Wah, Steve Branson, Peter Welinder, Pietro Perona, and Serge Belongie. The caltech-ucsd birds-200-2011 dataset. 2011.
- [36] Haofan Wang, Zifan Wang, Mengnan Du, Fan Yang, Zijian Zhang, Sirui Ding, Piotr Mardziel, and Xia Hu. Score-cam: Score-weighted visual explanations for convolutional neural networks. In *Proceedings of the IEEE/CVF conference on computer vision and pattern recognition workshops*, pages 24–25, 2020.
- [37] Eric Wong, Shibani Santurkar, and Aleksander Madry. Leveraging sparse linear layers for debuggable deep networks. In *International Conference on Machine Learning*, pages 11205–11216. PMLR, 2021.
- [38] Zhiyu Zhu, Zhibo Jin, Jiayu Zhang, and Huaming Chen. Enhancing model interpretability with local attribution over global exploration. In *Proceedings of the 32nd ACM International Conference on Multimedia*, pages 5347–5355, 2024.

A Additional Experiment and Results

A.1 Implementation Details

We used Resnet50 as the backbone, which extracts 2048 features. We project these features into 512 features before global pooling, i.e., $d_f = 512$. Based on our experiment and set of hyper-parameters, for the CUBs dataset, the $d_c = 2954$ and Stanford Cars $d_c = 3092$ are chosen. As the DBSCAN is used for clustering inside of each class, for each part and class, the number of clusters is not fixed.

The $\mathcal{L}_{bl}[32]$ loss also is

$$\mathcal{L}_{bl} = \mathcal{L}_{cond} + \mathcal{L}_{equi} + \mathcal{L}_{pres}, \quad (8)$$

where the objectives for each loss are:

- \mathcal{L}_{cond} : Each detected part should consist of a condensed and contiguous image region.
- \mathcal{L}_{equi} : encourages the equivariance of the attention maps in for input images and their augmented version (translation, rotation or scaling).
- \mathcal{L}_{pres} : All parts should be present at least in some of the images in the batch to avoid finding non-relevant parts.

A.2 Additional Ablation Studies

A.2.1 Effect of Hyper-parameters. We investigate the sensitivity of our model to the hyper-parameters α and β , which control the strength of the concept consistency and interpretability regularization terms, respectively. As shown in Fig. 8, our model remains robust across a wide range of values. Specifically, the classification accuracy (C Acc) and faithfulness score $F(n)$ exhibit stable trends, with peak performance achieved around $\alpha = 1.5$ and $\beta = 2.0$. This indicates that PCMNet effectively balances accuracy and interpretability without requiring extensive hyper-parameter tuning. The consistency of the scores across different settings highlights the reliability of the proposed regularization components.

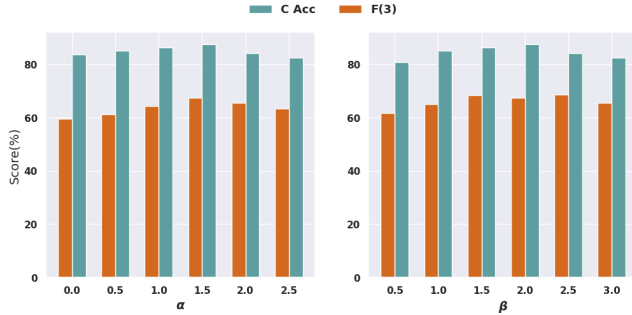


Figure 8: Impact of hyper-parameters α and β on classification accuracy (C Acc) and faithfulness score $F(3)$. Our method maintains strong performance across a wide range of values, showing robustness and stability in both predictive accuracy and interpretability.

Also, in Fig. 9, we evaluate the impact of hyperparameters in Eq.4 on classification accuracy. At first, we set $m_2 = 1$ and measure the effect of m_1 by gradually increasing the values. Once it is found, we search for m_2 . The best performance is achieved when m_1 is

set to 0.3 and m_2 to 1.5, respectively. The upward trend of the bars demonstrates the effectiveness of each loss.

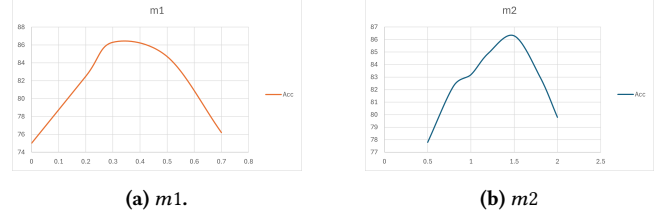


Figure 9: The model's classification accuracy in different values of m_1 and m_2 .

A.2.2 Effect of Non-Prototypical Concepts. To evaluate the impact of different concept vector types on model performance and interpretability, we conduct an ablation study using prototypical (z^i) and non-prototypical (g^i) concept vectors. As shown in Table 4, using only non-prototypical vectors significantly reduces both classification accuracy and faithfulness scores. In contrast, employing only prototypical vectors retains higher classification performance and strong concept-based faithfulness. The full PCMNet, which combines both concept types, achieves the best results across both datasets, suggesting that the interplay between prototypical and non-prototypical representations enhances both prediction accuracy and interpretability.

CAVs	Cars		Birds	
	C Acc	F(1)-F(5)	C Acc	F(1)-F(5)
Baseline	84.1	1.54 - 6.61	83.2	1.21-5.56
PCMNet + Prototypical	86.2	61.8 - 92.63	84.5	56.8 - 87.4
PCMNet + Non-Prototypical	79.4	42.80 - 75.73	78.15	35.9 - 67.7
PCMNet (Full)	87.5	59.33 - 91.73	86.0	55.7 - 87.3

Table 4: Impact of prototypical (z^i) and non-prototypical (g^i) concept vectors on PCMNet's classification accuracy (C Acc) and faithfulness scores (F(1)-F(5)) on Cars and Birds datasets. The full model achieves superior performance, highlighting the benefit of combining both concept types.

A.3 Additional Qualitative Results

More results of the PCMNet prototypical concept are shown in Figs. 10 and 11. 12 illustrates examples of non-prototypical concepts discovered by our model for the Cars (left) and CUBs (right) datasets. For each dataset, the concept location on a test image is highlighted with a green bounding box, while corresponding activations in training examples are shown on the right using red bounding boxes. These concepts provide complementary cues to prototypical ones. For example, in the first row of Cars, the "cargo" attributes are not well represented in prototypical concepts since they appear in a small subset of vehicles, yet they are highly discriminative for decision-making. Similarly, the last row in CUBs shows the "webbed feet" concept, which is especially relevant and explainable for Albatross species, while foot prototypes are not sufficiently distinctive across the dataset. These findings highlight



Figure 10: Visualization of activated concepts in test data and showing some examples in the training set for StanfordCars datasets. Each concept is shown with an index and percentage of explanation for the model decision.

the value of incorporating non-prototypical concepts in improving both interpretability and robustness of the model.

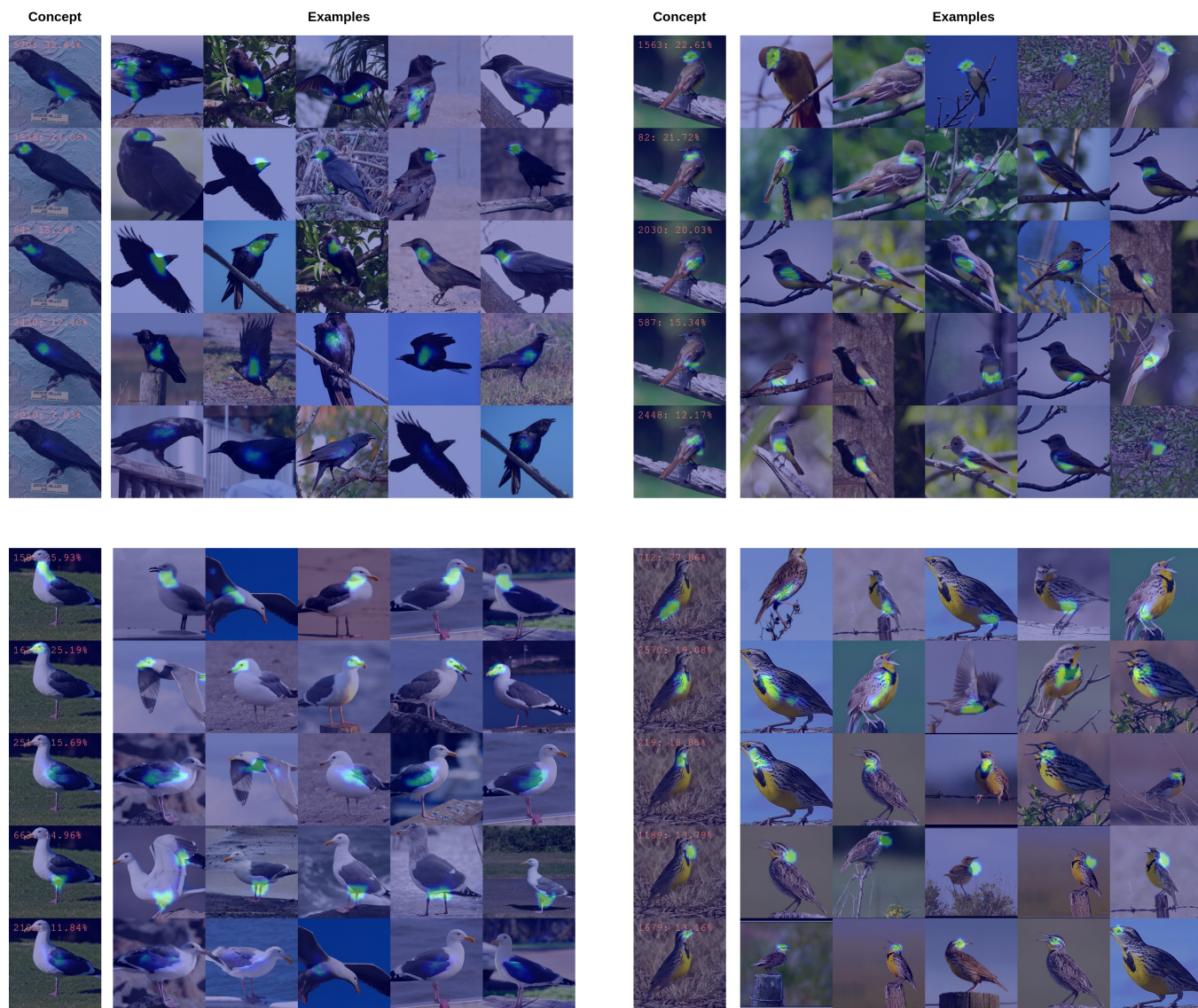


Figure 11: Visualization of activated concepts in test data and showing some examples in the training set for CUB-200 Birds datasets. Each concept is shown with an index and percentage of explanation for the model decision.

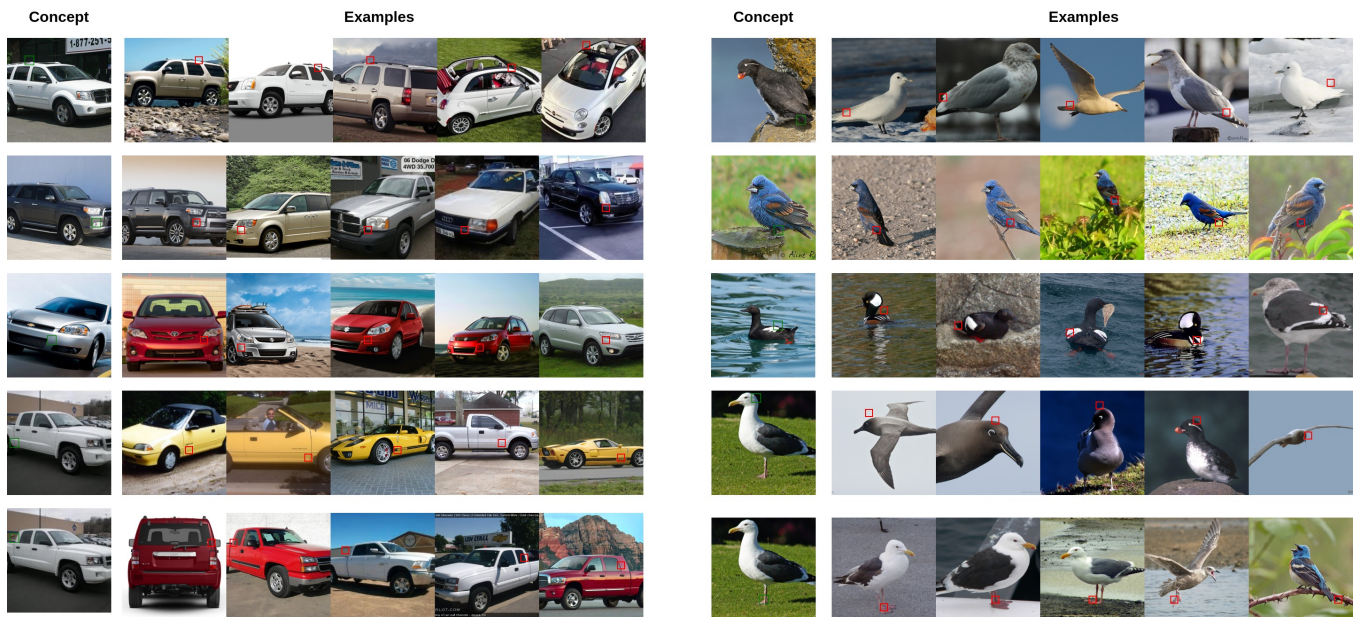


Figure 12: Visualization of non-prototypical activated concepts in test data and showing some examples in the training set for (left) Stanford Cars and (right) CUB-200 Birds datasets. Similar to ProtoPNet and PIPNet, we select the patch for the region of the activated concept.

Paper Title

001

Supplementary Material

002

arXiv:2504.12197v1 [cs.CV] 16 Apr 2025

A. Additional Experiment and Results

A.1. Implementation Details

We used Resnet50 as the backbone, which extracts 2048 features. We project these features into 512 features before global pooling, i.e., $d_f = 512$. Based on our experiment and set of hyper-parameters, for the CUBs dataset, the $d_c = 2954$ and Stanford Cars $d_c = 3092$ are chosen. As the DBSCAN is used for clustering inside of each class, for each part and class, the number of clusters is not fixed.

The $\mathcal{L}_{bl}[\cdot]$ loss also is

$$\mathcal{L}_{bl} = \mathcal{L}_{cond} + \mathcal{L}_{equi} + \mathcal{L}_{pres}, \quad (1)$$

where the objectives for each loss are:

- \mathcal{L}_{cond} : Each detected part should consist of a condensed and contiguous image region.
- \mathcal{L}_{equi} : encourages the equivariance of the attention maps in for input images and their augmented version (translation, rotation or scaling).
- \mathcal{L}_{pres} : All parts should be present at least in some of the images in the batch to avoid finding non-relevant parts.

A.2. Additional Ablation Studies

A.2.1. Effect of Hyper-parameters

We investigate the sensitivity of our model to the hyper-parameters α and β , which control the strength of the concept consistency and interpretability regularization terms, respectively. As shown in Fig. 1, our model remains robust across a wide range of values. Specifically, the classification accuracy (C Acc) and faithfulness score $\mathbf{F}(n)$ exhibit stable trends, with peak performance achieved around $\alpha = 1.5$ and $\beta = 2.0$. This indicates that PCMNet effectively balances accuracy and interpretability without requiring extensive hyper-parameter tuning. The consistency of the scores across different settings highlights the reliability of the proposed regularization components.

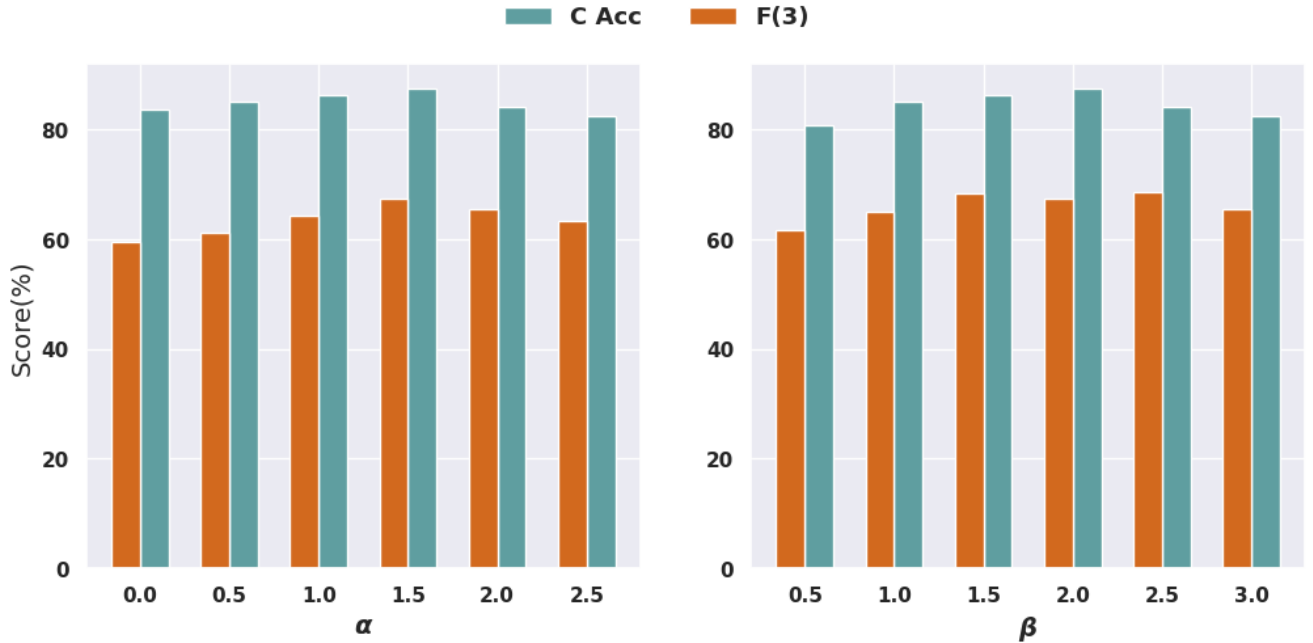


Figure 1. Impact of hyper-parameters α and β on classification accuracy (C Acc) and faithfulness score $\mathbf{F}(3)$. Our method maintains strong performance across a wide range of values, showing robustness and stability in both predictive accuracy and interpretability.

Also, in Fig. 2, we evaluate the impact of hyperparameters in Eq.?? on classification accuracy. At first, we set $m_2 = 1$ and measure the effect of m_1 by gradually increasing the values. Once it is found, we search for m_2 . The best performance is achieved when m_1 is set to 0.3 and m_2 to 1.5, respectively. The upward trend of the bars demonstrates the effectiveness of each loss.

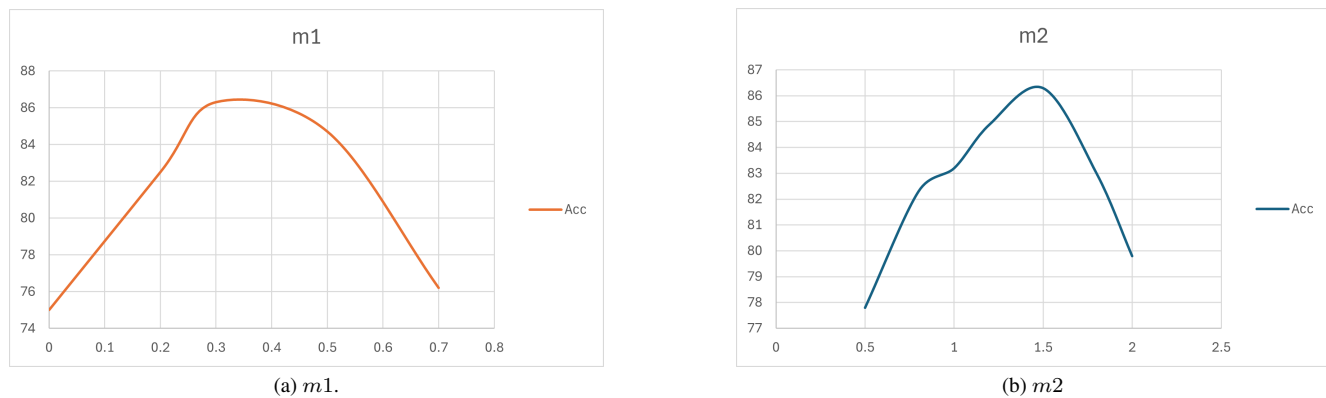
Figure 2. The model's classification accuracy in different values of $m1$ and $m2$.

Figure 3. Visualization of activated concepts in test data and showing some examples in the training set for StanfordCars datasets. Each concept is shown with an index and percentage of explanation for the model decision.

A.2.2. Effect of Non-Prototypical Concepts

To evaluate the impact of different concept vector types on model performance and interpretability, we conduct an ablation study using prototypical (z^1) and non-prototypical (g^1) concept vectors. As shown in Table 1, using only non-prototypical vectors significantly reduces both classification accuracy and faithfulness scores. In contrast, employing only prototypical vectors retains higher classification performance and strong concept-based faithfulness. The full PCMNet, which combines both concept types, achieves the best results across both datasets, suggesting that the interplay between prototypical and non-prototypical representations enhances both prediction accuracy and interpretability.

A.3. Additional Qualitative Results

More results of the PCMNet prototypical concept are shown in Figs. 3 and 4. 5 illustrates examples of non-prototypical concepts discovered by our model for the Cars (left) and CUBs (right) datasets. For each dataset, the concept location on a test image is highlighted with a green bounding box, while corresponding activations in training examples are shown on the right using red bounding boxes. These concepts provide complementary cues to prototypical ones. For example, in the first row of Cars, the "cargo" attributes are not well represented in prototypical concepts since they appear in a small subset of vehicles, yet they are highly discriminative for decision-making. Similarly, the last row in CUBs shows the "webbed feet" concept,

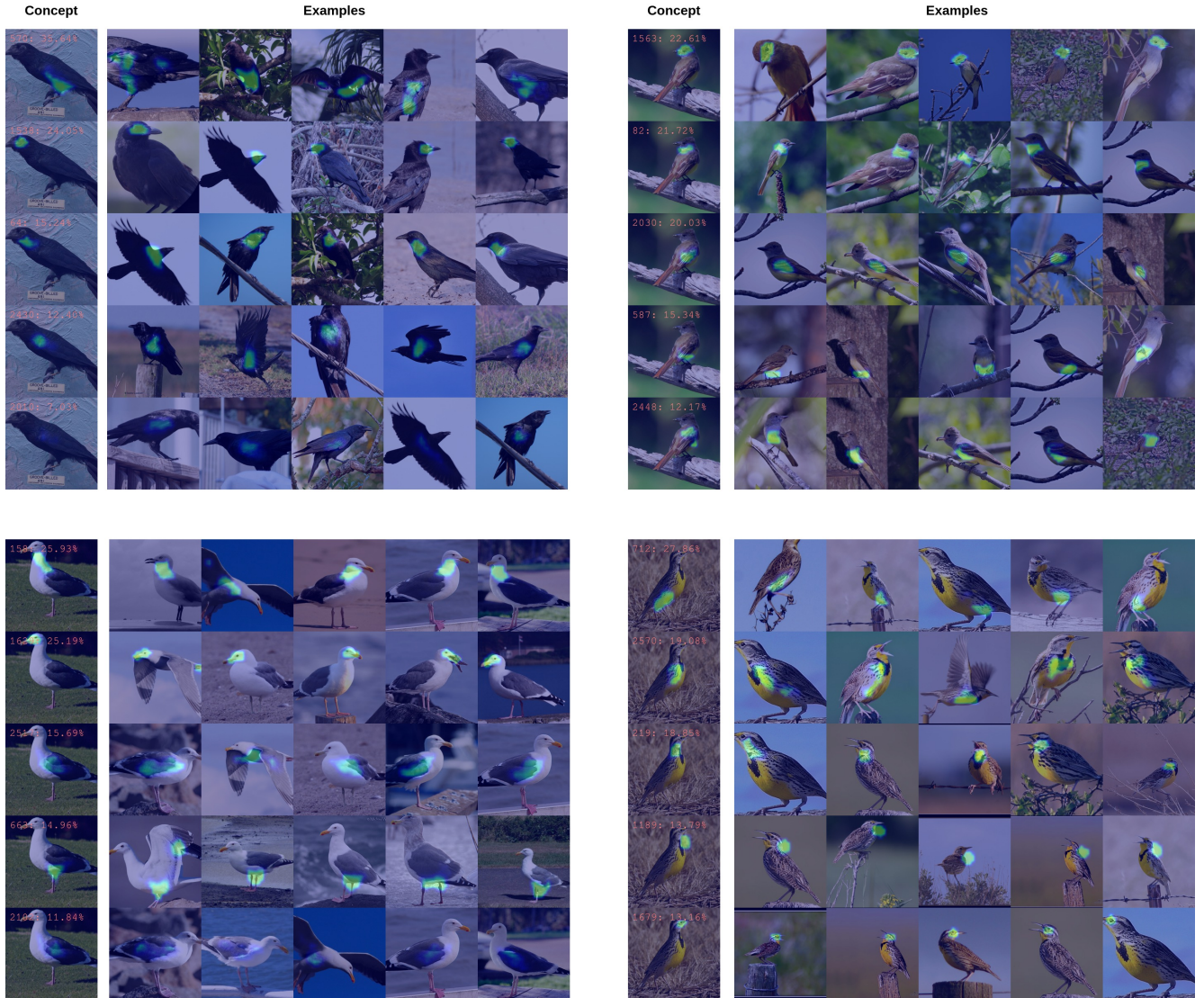


Figure 4. Visualization of activated concepts in test data and showing some examples in the training set for CUB-200 Birds datasets. Each concept is shown with an index and percentage of explanation for the model decision.

CAVs	Cars		Birds	
	C Acc	F(1)-F(5)	C Acc	F(1)-F(5)
Baseline	84.1	1.54 - 6.61	83.2	1.21-5.56
PCMNet + Prototypical	86.2	61.8 – 92.63	84.5	56.8 - 87.4
PCMNet + Non-Prototypical	79.4	42.80 – 75.73	78.15	35.9 - 67.7
PCMNet (Full)	87.5	59.33 – 91.73	86.0	55.7 - 87.3

Table 1. Impact of prototypical (\mathbf{z}^i) and non-prototypical (\mathbf{g}^i) concept vectors on PCMNet’s classification accuracy (C Acc) and faithfulness scores (F(1)-F(5)) on Cars and Birds datasets. The full model achieves superior performance, highlighting the benefit of combining both concept types.

which is especially relevant and explainable for Albatross species, while foot prototypes are not sufficiently distinctive across the dataset. These findings highlight the value of incorporating non-prototypical concepts in improving both interpretability and robustness of the model.

042
043
044

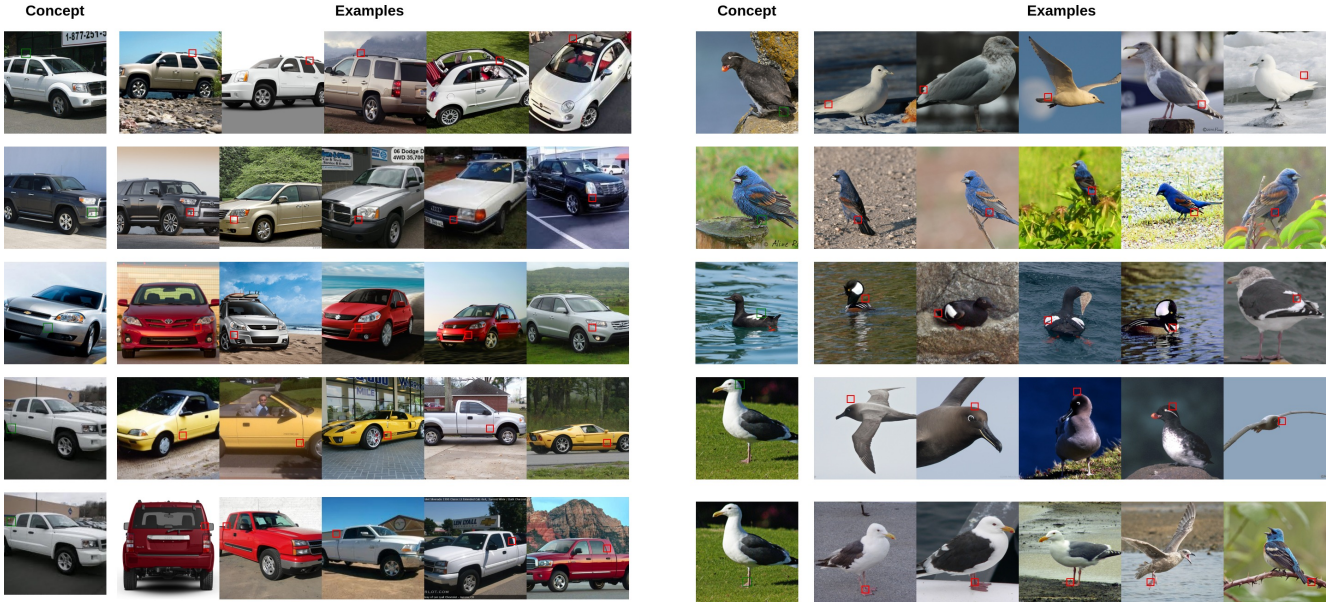


Figure 5. Visualization of non-prototypical activated concepts in test data and showing some examples in the training set for (left) Stanford Cars and (right) CUB-200 Birds datasets. Similar to ProtoPNet and PIPNet, we select the patch for the region of the activated concept.